# Thermophysical behavior of diamond composites for diode laser heat sink applications at temperatures between 4 K and ambient

C. Edtmaier[1], E. Bauer[2], J. Segl[3], and A. Foelske-Schmitz[4]
*TU Wien,Vienna, 1040, Austria*

L. Pambaguian[5]
*ESA-ESTEC, Noordwijk, 2200 AG, The Netherlands*

**In the frame of an ESA Basic Research Technology Program (TRP) activity experimental work was performed on "clean model" systems, i.e. well-defined synthetic diamond mono-crystal surfaces, which were functionalized and characterized by XPS. In a second approach those results were transformed onto synthetic diamond particles in Al- and Ag-diamond composites and the measurement of thermal conductivity in the temperature range between roughly 4 K and 298 K. Knowledge of thermal transport between diamond and metal surfaces and the thermal conductivity behavior of composites in that temperature range is essential for the development of improved thermal management applications and of heat sink materials to be operated in cryo-lasers and in space LIDAR applications and similar. The results obtained show an influence of matrix composition, diamond particle size and diamond surface treatment on thermal conductivity behavior, which can be as high as 1050 W $m^{-1}$ $K^{-1}$ at around 150 K. The surface treatment results in oxygenated diamond surfaces and can influence interfacial thermal conductance *h*. Furthermore, the *h*(T)-values in our findings on "real" composites can be close to values determined on clean model systems, i.e. sputtered and evaporated metal layers on even diamond mono-crystal substrates. In a next approach laser crystal materials were directly joined to the heat sink material to minimize strains.**

## Nomenclature

| | | |
|---|---|---|
| $\kappa$ | = | thermal conductivity |
| $Q$ | = | heat flux |
| $T$ | = | temperature |
| $\Delta T$ | = | temperature difference |
| $h$ | = | interface thermal conductance |
| $f$ | = | volume fraction |
| $\varphi$ | = | phase contrast |
| $a$ | = | inclusion size |
| $A$ | = | surface of the sample; amplification factor |
| $\varepsilon$ | = | emissivity |
| $L$ | = | length |

[1] Ass. Prof., Institute of Chemical Technologies and Analytics, Getreidemarkt 9/164-CT, 1060 Wien, christian.edtmaier@tuwien.ac.at.
[2] Prof. for Solid State Physics, Institute of Solid State Physics, Wiedner Hauptstr. 8, 1040 Wien, ernst.bauer@tuwien.ac.at.
[3] Researcher, Institute of Chemical Technologies and Analytics, Getreidemarkt 9/164-CT, 1060 Wien, jakob.segl@tuwien.ac.at
[4] Head Analytical Instrumentation Center TU Wien, Getreidemarkt 9, 1060 Wien, annette.foelske-schmitz@tuwien.ac.at
[5] Engineer - Materials Technology Section Product Assurance and Safety Department, Keplerlaan 1, TEC-QTM #Ef074 - PO Box 299, laurent.pambaguian@esa.int.

## I. Introduction

Stringent thermal requirements of future space missions, especially for devices of instruments having high heat dissipation rates in conjunction with a very accurate temperature control in the order of some tenths of a degrees require advances in thermal management technology and materials used for their implementation. In this context, a crucial need exists for the availability of novel thermally high conductive materials and structures ("heat spreaders") in combination with advanced thermal control technologies such as two-phase heat transport systems.

Because of the progress in the ultra-large-scale-integration of ICs, microelectronic components and devices are becoming more compact, demanding advances in advanced thermal management. Current ICs for microprocessors operated at high frequencies are routinely characterized by power densities on the order of tens of W $cm^{-2}$. Such large densities lead to highly localized heating ("hot spots") and subsequent hazard to failure. Laser transmitters and their components such as laser diodes are further typical examples for such thermal requirements, since the laser wave length emitted from space LIDAR (Light Detection And Ranging) strongly depends on the temperature of the laser diodes.

A number of laser-based instruments are under space qualification and flight approval for near-term ESA missions, i.e. Aeolus/ALADIN, EarthCARE/ATLID and MERLIN. NASA-GSFC is actively pursuing laser-based altimetry and atmospheric LIDAR methods for earth and planetary remote sensing instruments (Calipso, GLAS, MOLA, MLA). Almost all the laser and LIDAR instruments being considered by NASA and ESA rely on conductively cooled, diode-pumped solid state lasers as their transmitter source. Solid state lasers, currently Nd:YAG-type, are optically pumped by High-Performance Laser Diodes, arranged in an Array (LDA) [4]. FULAS, ESA's actual diode laser demonstrator program, aims at developing a space compatible diode laser technology suited for adaptation to different future missions (if possible). Performance of solid state lasers and LDAs is highly impacted by temperature variations. Therefore, the laser based instruments request for highest quality thermal control and a careful selection of materials. Miniaturization of microelectronic circuits and LDA impose tremendous challenges on material selection for thermal management and packaging that ensure effective thermal dissipation and compatible thermal expansion for best possible thermal control.

The idea of operating lasers at low temperatures is not new: the second laser in history was a cryogenic one. While this concept was originally used just because room-temperature operation was hard to achieve, a renewed interest in cryogenic operation for high-power lasers and amplifiers emerged, as a number of the detrimental thermal effects such as depolarization loss, thermal lensing or even fracture of the laser crystal can be a real problem limiting the performance. Such effects may be effectively suppressed by cryogenic cooling of the gain medium to temperatures such as 77 K, or even 4 K, as thermal conductivity of the gain medium increases, mainly because the mean free path length of phonons increases. As an example, the thermal conductivity of YAG increases by a factor of 7 when the temperature is reduced from 300 K to 77 K. Furthermore, the coefficient of thermal expansion (CTE) is decreased at low temperature, which reduces thermal lensing from bulging and stress and the tendency for stress fracture. The thermooptic coefficient is decreased, further lessening thermal lensing. The laser and absorption cross sections of rare earth ions are increased, thus, saturation powers are reduced, and the laser gain is increased. Consequently, the threshold pump power is abated, and shorter pulses can be obtained. The combination of such factors may allow strong improvements in laser performance and thus generating much higher laser output powers without excessive thermal effects. As a matter of fact, cryogenic laser cooling will induce increasing system complexity. To decrease mass of instruments and components and avoid complexity, respectively, the use of heat sink materials, that are thermally extremely high conductive and have a CTE better matching that of the heat source, is essential.

### A. Technical Background

Monolithic materials cover a wide range of combinations of CTE and thermal conductivity; however, the required combination of highest thermal conductivity (TC) and lowest CTE is virtually not occupied. The most promising class of materials to reach thermal conductivity beyond that of copper or silver are metal matrix composites (MMCs) containing diamonds. Although these materials have received some interest since the early 90's, most are still at scientific level, only few companies commercialized such products.

Unfortunately, the diamond/metal contacts have a finite interface thermal conductance (ITC, or TBC, thermal boundary conductance). Even if perfect mechanical bonding is achieved at the interface, intrinsic interface thermal resistance (ITR) arises due to the scattering of phonons and electrons when travelling between materials with different elasticity and dielectric constants. The presence of limited heat flow across interfaces resulted in significant large body of work to improve bonding between matrix and inclusion phases and therefore heat transfer across the interface which may thus give access to an overall improved thermal conductivity of the composites.

On an application level, this is achieved by either introducing carbide forming elements to form stronger chemical and physical bonds at the interface [5-10], increasing the effective contact surface between metal and inclusion [11] or by varying the composite fabrication parameters [12]. One less exploited aspect concerns the role of surface termination of diamond surfaces by oxygenation or hydrogenation on the Kapitza resistance and subsequently on the thermophysical properties of diamond MMCs [3, 13-15]. From a scientific perspective, it is essential to understand how this interface has to be designed in order to minimize the Kapitza resistance and to improve the TBC.

Physical bond between the constituents is of special interest when using the best thermal conductors, i.e. copper and silver, as a matrix metal. Both are known not to wet and bond to carbon allotropes, but improved wetting and bonding was observed after alloying with carbide formers. Aluminum as matrix metal steadily forms carbides, $Al_4C_3$; excessive formation is undesirable, as it has low thermal conductivity and readily corrodes in moist air to form aluminas, such as $Al(OH)_3$. It is well known, that $Al_4C_3$ formation can be controlled by alloying Al with Si, as a result of competitive formation of SiC.

For non-wetting systems interlayers are produced by two different methods: using alloys instead of pure matrices and by coatings, respectively. Alloying elements must have a certain affinity to carbon, thus carbide forming elements (Mo, W, Cr, Si,...) are favored. Note, that alloying additives being present in a matrix metal may cause a severe reduction in matrix thermal conductivity by the formation of a solid solution. This degradation can be significant, as 0.2 wt% of Ti in Cu reduces the thermal conductivity by about one-fifth. Conversely the additions of V, Cr, Ti or Si in Cu result in significant reductions in contact angles with carbon, 0.2 at% Cr in Cu causes a contact angle of 40° compared to 125° for pure Cu with vitreous carbon [16, 17]. Furthermore, the interlayer can be generated by pre-coating the inclusion phase with carbide forming elements, i.a. by methods like PVD. Such pre-coated inclusions are contacted with the matrix metal in a subsequent step (e.g. by infiltration techniques or hot-pressing).

The idea behind micro-structuring is to increase the effective contact areas in order to decrease the local heat flux. As commonly accepted, the contact area cannot be simply increased by decreasing the size of the inclusions. Decreasing size of inclusions stringently leads to a deterioration of composite thermal properties. To give an example, when considering C-nanotube inclusions in composite materials, the composite thermal conductivity is fairly low due to large interfacial resistance, although C-nanotubes are considered to be the most thermally conductive material. Using large sized inclusions (diamonds) will maintain the large mean free phonon path, and the local heat flux can be minimized by micro-structured inclusion surfaces, details in Figure 1.

The role of surface termination of diamond surfaces by oxygenation or hydrogenation on the Kapitza resistance

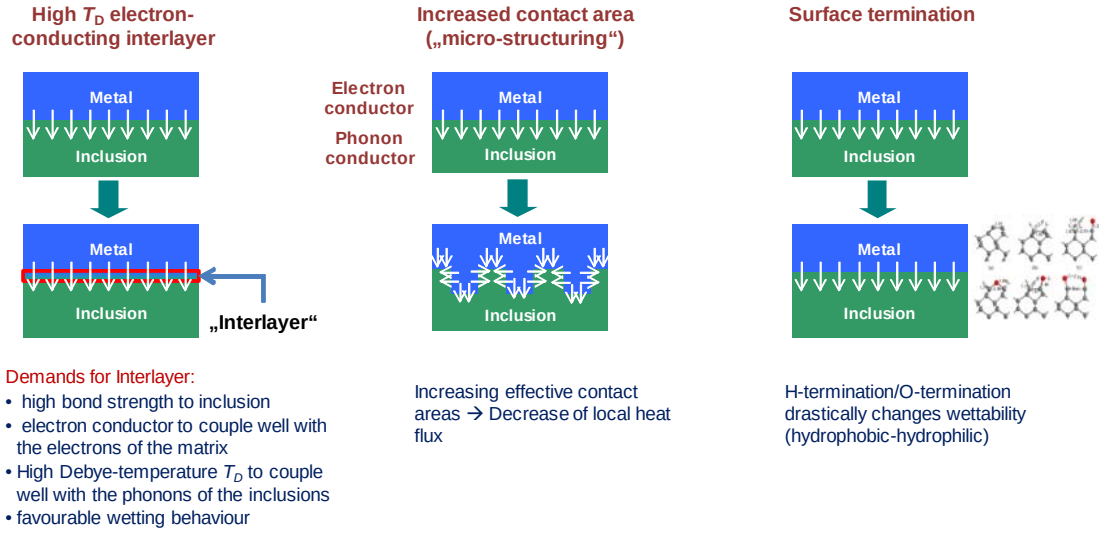


**Figure 1. Possibilities to influence the interface in diamond/metal contacts in order to minimize the interfacial resistance (Kapitza-resistance) either by interlayers, micro-structuring of the inclusion surfaces (increasing the contact area) and the surface termination of the inclusions, respectively.**

and subsequent on the thermophysical properties of diamond MMCs may play an important role in the resulting thermophysical properties of diamond composites, as a clear difference in TBC between oxygen and hydrogen terminated diamond surfaces had been determined [3, 18, 19].

To conclude from the state of the art presented above is that thermal boundary conductance between a metal with a low Debye-temperature, i.e. silver or copper, and a dielectric with very high Debye-temperature, i.e. diamond, could be improved by following different concepts (Figure 1):

a) A layer of electron-conducting material (to couple well with electrons of the matrix) is introduced at the interface between the two phases that has itself a high Debye-Temperature to couple well with the phonons of the inclusions, forms epitaxial on the diamond, has a high bond strength with the diamond and the metal, and has favorable wetting behavior.
b) Increasing the specific surface by introducing roughness at a length scale that is large compared to the phonon mean free path (on the order of 100 nm) and the dominant wavelength at room temperature (a few nanometers) should also improve the effective interface thermal conductance.
c) Surface termination of diamond surfaces by oxygenation or hydrogenation.
d) Any combination of a), b), and c), respectively.

**B. Predictive schemes for thermal conductivity**

Generally predictive schemes for physical properties of two- or even multi-phase materials are an important tool for assessing the potential of, and then tailoring, composite materials for specific applications. There are several predictive schemes for thermal conductivity described in literature, amongst the most powerful is the differential effective medium (DEM) scheme. The thermal conductivity of two-phase materials can be predicted by needs to take into account the finite value of the interface thermal conductance between the two solid phases. Analytically, this is typically solved by replacing the inclusion with a non-ideal interface by an ''effective'' inclusion having an effective conductivity $\kappa_i^{eff}$ given by

$$\kappa_i^{eff} = \frac{\kappa_i}{1 + \frac{\kappa_i}{ah}} \tag{1}$$

where $\kappa_i$ is the intrinsic thermal conductivity of the disperse (inclusion) phase, $a$ is the radius of the inclusion idealized as a sphere and $h$ is the interface thermal conductance, defined as the ratio of heat flux and temperature drop across the interface. The leading equations for the DEM approach of spherical inclusions had been developed by Tavangar[9], leading to the implicit relation between a conductivity amplification factor $A = \kappa_c/\kappa_m$ and the effective phase contrast $\varphi^{eff} = \kappa_i^{eff}/\kappa_m$. $f_i$ is the volume fraction of the inclusion phase, more details given in [9]:

$$(1 - f_i) = \frac{\varphi^{eff} - A}{\varphi^{eff} - 1} A^{-1/3} \tag{2}$$

Thermal interface conductance values $h$(T) were previously reported between diamond and metals [3, 20, 21] and other substrates like sapphire, $BaF_2$ and MgO or in metal/metal interfaces [22]. The room temperature TBC values between metal/dielectric interfaces and metal/metal interface span two orders of magnitude, $1–300\times10^7$ W m$^{-2}$ K$^{-1}$. Measurements at different temperatures show a decrease in TBC with decreasing temperature, but differences between different bibliographic references are evident (compare data of Stoner-Maris [23], Monachon-Weber [3, 24] and Collins [13]). The direct experimental determination of TBC values is not easy, as it needs elaborate experimental set-up and equipment (time domain thermoreflectance, TDTR): the experimental setup is a pump-probe femtosecond-laser arrangement in which the pump is used to heat the sample surface of a sputtered layer of metal on a plane diamond substrate, and the probe to measure the reflectivity of the sample surface.

An alternative method is to measure thermal conductivities of MMCs with different sized diamonds, that allows to assess TBC, as it can be calculated using the leading equations for the DEM approach: rearranging Eq. (2) and resolving for $\kappa_i^{eff}$, the effective inclusion conductivity leads to

$$\kappa_i^{eff} = \kappa_m \left[ \frac{1 - f_i - A^{2/3}}{1 - f_i - A^{-1/3}} \right] \tag{3}$$

Experimental determination of the thermal conductivities $\kappa_c$(T) and $\kappa_m$(T) easily allows calculating $\kappa_i^{eff}$(T), Eq. (3), for MMCs using different diamond grit sizes. When plotting $1/\kappa_i^{eff}$ versus $1/a$ a straight line should follow, and

from this, in turn, $h$ and $\kappa_i$ can be deduced from the slope and the intersect at $1/a = 0$, respectively ("inverse method", see also [25]).

## II. Experimental Procedure

Diamond single crystals (100) of 3 mm × 3 mm × 1 mm size (purchased by E6, Germany) were defined as a clean model system to study the influence of surficial functionalization on thermal conductivity. In the past it was shown, that diamond functionalization can be easily done by wet chemical methods [26, 27], thus the monocrystals were treated to functionalize the surface with oxygen groups by reflux cooking in 20 mL of $H_2SO_4$ and aqua regia, respectively, for 3 hours, before the monocrystals were rinsed with distilled water and blown dry by $N_2$ gas. Although the as-delivered diamonds are natively hydrogen terminated, they were subjected to annealing operation in a furnace of 500 °C under a constant flow of hydrogen gas for 60 min to guarantee defined hydrogenation of the diamond surface. Before introducing the diamonds into the hot furnace, it was first flushed with argon gas subsequently the gas was switched to hydrogen. The furnace was then switched off and the samples were furnace cooled to ambient.

In order to avoid any contaminations, the specimens were immediately inserted into the XPS device to get a qualitative view of functionalization. XPS data was collected by SPECS XPS/UPS system under ultra-high vacuum conditions (<$10^{-8}$ Torr). A monochromatic X-ray source (µ-Focus 350, Al Kα) allows focusing the X-ray beam to diameters between 500 µm and 40 µm. The analyzer system consists of a Phoibos 150 hemispherical energy analyzer with wide angle lens (WAL) and 2D delay-line detector that allows detection of kinetic energy of photoelectrons in parallel to the angle dependent information of each measurement. The acceptance angle is 60° (resulting in emission angles from 20° to 80° with respect to the normal of the sample surface). The XPS system is regularly calibrated using the Ag $3d_{5/2}$, the Cu $2p_{3/2}$ and the Au $4f_{7/2}$ lines of sputter cleaned samples as reference signals.

The source was operated at a power of 88 W (8 mA, 11 kV) using a beam diameter of 500 µm. Survey spectra were recorded using a pass energy of 100 eV and 0.5eV steps and high resolution spectra using a pass energy of 80 eV and 0.05eV steps, respectively. To compensate for charging effects, the maxima of the angle integrated C1s peaks were shifted to a binding energy (BE) of 285.2 eV[28, 29]. The data was evaluated using the CASA XPS software (v. 2.317dev6.7e, *Casa Software Ltd.*). Background subtraction was performed according to Shirley[30]. Atomic sensitivity factors according to Scofield[31] as implemented in the CASA XPS data base were used for quantification.

Composites were produced by liquid metal infiltration (LMI) of Al, Al–Si and Ag–Si base material into a tapped and vibrated powder bed of synthetic diamond grit of mesh sizes 70/80, 230/270 and 500/600. The matrix alloy was primarily inductively melted and cast using 3N8 Al, 4N Ag and 4N Si base elements. Along with the composites, a sample of same geometry yet without diamond was produced as well. The matrix conductivity was investigated by electrical resistivity on Ag–xSi for x = 0.005, x = 0.01 and x = 0.03 and x = 0 and x = 0.03 in Al–Si respectively to identify optimal matrix compositions.

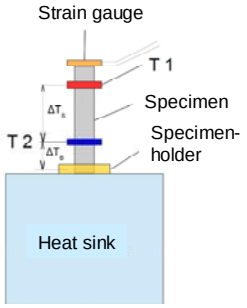


**Figure 2. Schematic experimental setup for thermal conductivity**

The synthetic (Ib-) diamonds were of the MBD4 type (purchased from Luoyang High-Tech Qiming Superhard Materials Co. Ltd., Luoyang, Henan, China). Diamond particles were also oxygen surface terminated by similar operations described above, i.e. immersing in hot aqua regia (3:1, 32% HCl, 53% $HNO_3$) and $H_2SO_4$ respectively for 3 hours, subsequently rinsed with de-ionized water and 2-propanol and finally dried at 70 °C. From pre-studies it was known that aqua regia treatment is superior for Ag/diamond composites, whereas $H_2SO_4$ treatment seems to be beneficial for Al/diamond composites. Both procedures are expected to produce oxidized diamond surfaces, samples undergoing such method are denoted as Ag(Al)-xSi/O/diamond.

The thermal conductivity samples were infiltrated net-shape. After the infiltration temperature of roughly 1400 K (Ag/diamond composites) and 1150 K respectively (Al/diamond composites) was reached, the system was allowed to thermally equilibrate for about 5 min. Argon gas pressure was applied up to 4 MPa. The heating was switched off after 5 min and the infiltrated body was furnace cooled within < 30 min to room temperature. After cool down, composite pieces were dismantled from the die.

The volume fraction diamond in the composite was determined for all composites by densitometry to be 64 and 62 vol.% for the composites from largest (mesh 70/80) to the smallest (mesh 500/600) sized diamond composites. Heat treatment operation on all samples was performed before thermal conductivity measurements according optimal time/temperature schemes and may guarantee minimum dissolved Si in the Ag and Al lattice by favoring the formation of Si precipitates. Heat treatment operations were performed in a furnace under Ar atmosphere at 550 °C/2h and 250 °C/12h (Al–Si) and 830 °C/2h and 500 °C/20h (Ag–Si), pure Al and its composites were not heat treated.

Temperature dependent thermal conductivity measurements were performed in a steady-state heat flow equipment in the temperature range of 4 K up to ambient temperature using a $^4$He flow cryostat. Sample size is a rod of 2 mm diameter and an overall length of 12 to 15 mm. One end of the sample is anchored onto a thick copper panel mounted on the heat exchanger of the system (cryostat), whereas a strain gauge is glued on the other end to electrically establish the necessary temperature gradient (Figure 2). The employed energy - and from this the heat flux Q - can be derived from the electrical current and by the voltage drop of the strain gauge. The temperature evolution along the sample length $L$ is controlled by means of Au–0.07 Fe (at.%) vs. Chromel differential thermocouples, which derives its reference temperature by Pt and Ge resistive temperature sensors, fixed on the heat sink. Thermal conductivity data can be easily calculated by the relationship $\kappa = Q \cdot L/(A \cdot \Delta T_s)$, with $\Delta T_s = T_2 - T_1$ (see Figure 2).

Employing a 4 point a.c. technique, the absolute values of the electrical resistivity for Al–Si and Ag–Si matrix alloys can be obtained. Samples of about 1 mm × 1 mm × 10 mm are electrically contacted by thin gold wires (diameter 50 µm) using spot welding and fixed on a small sample platform which can be connected directly with the sample holder. A modified a.c. bridge (Lakeshore AC370) is used to measure the resistance of the sample in the context of a geometrical factor (i.e., cross section and length between voltage contacts) the material dependent specific electrical resistivity can be measured. Putting the sample holder into a bath cryostat allows deriving the electrical resistivity as a function of temperature from about 4 K to 300 K. Temperature dependent electrical resistivity data can help to better understand the respective thermal conductivity since both quantities are interrelated via the Wiedemann-Franz law, stating that the same charge carriers responsible for the electrical transport are also responsible for the heat transport from the warm to the cold end of the sample. This relation enables to identify the electronic thermal conductivity $\kappa_e$ as part of the total thermal conductivity $\kappa$.

For the steady state heat flow method, which is used to measure thermal conductivity data, we assume that the uncertainty on the thermal conductivities measured is < 5 % over the whole range of temperatures.

## III. Results and Discussion

In a first approach we performed experimental work on "clean model" systems, i.e. well defined synthetic diamond mono-crystal surfaces, which were functionalized and characterized by XPS (section III B). We wanted to study the kind of functionalization by wet chemical treatments, as it appeared in the past, that thermal conductivity and interfacial thermal conductance can be largely enhanced by surficial treatments on diamond particles. To exclude effects from the somehow messier conditions in a gas pressure infiltration equipment, it was studied on such clean model system.

In a second approach those XPS results were transformed onto synthetic diamond particles in Al/ and Ag/diamond composites and the measurement of thermal conductivity in the temperature range between roughly 4 K and 298 K (section III D). The composites were reinforced with synthetic diamond particles of different sizes in order to vary the effective thermal conductivity of the inclusion phase and in the hydrogen-terminated (as delivered) and oxygen-terminated state (chemical treatment). Si as active elements needs to be added to improve the interface between matrix and inclusion. We furthermore investigated the properties of the unreinforced matrix (section III C).

We use the previously proven predictive capacity of the DEM scheme to calculate i) the theoretical and expected thermal conductivity behavior of Ag & Al/diamond composites (section III A), and ii) the TBC by the inverse method described above (section III D).

In an another task two selected laser crystal materials were directly joined to a diamond composite (heat sink) (section III E). Such bonding was performed during the infiltration process of the diamond beds to avoid brazing of a laser crystal material to a heat sink. It is known, that brazing with indium can cause delamination between the heat sink and the laser crystal due to their highly different coefficients of thermal expansion. This cause stresses, that may lead to cracks in the slab crystal. A diamond composite can have low CTE, mainly depending on diamond volume fractions, thus both, the CTE of the composite and the CTE of the laser crystal can match.

### A. Predicting thermal conductivity of diamond composites between 4 K and ambient by DEM approach

In Figure 3a, the DEM approach predicts the effective composite thermal conductivity of Ag/diamond and Ag–3Si/diamond composites in the temperature range of 4 K up to ambient. Calculations were performed using Equation (1) under the assumption of a volume fraction of 60% of diamonds of 200 µm size, which roughly correspond to mesh size 70/80.

We first notice the evolution of $\kappa$(T) of the pure substances Ag and diamonds, based on thermophysical data given by Haynes[1] and Hudson[2], and identify the typical behavior for pure metals with marked peak conductivity close to 10 K. The diamond thermal conductivity is different, as the maximum shifts to higher temperatures of about 80 K due to the higher Debye-temperature $T_D$ of diamond. In this context we would like to bring in mind, that the availa-

ble data for the thermal conductivity even for pure substances can be quite different, compare [1] and [32] for silver or [33], [34] for Al, Al-alloys and others. This might be attributed to dramatic changes in experimental techniques over the decades, and to general "intrinsic" difficulties of measurements and measurement setups leading to larger uncertainties in test results of the same substances. To get an idea of problems in thermophysical testing, we recommend the work of Pintsuk [35], who performed round-robin tests on CuCrZr heat sink material.

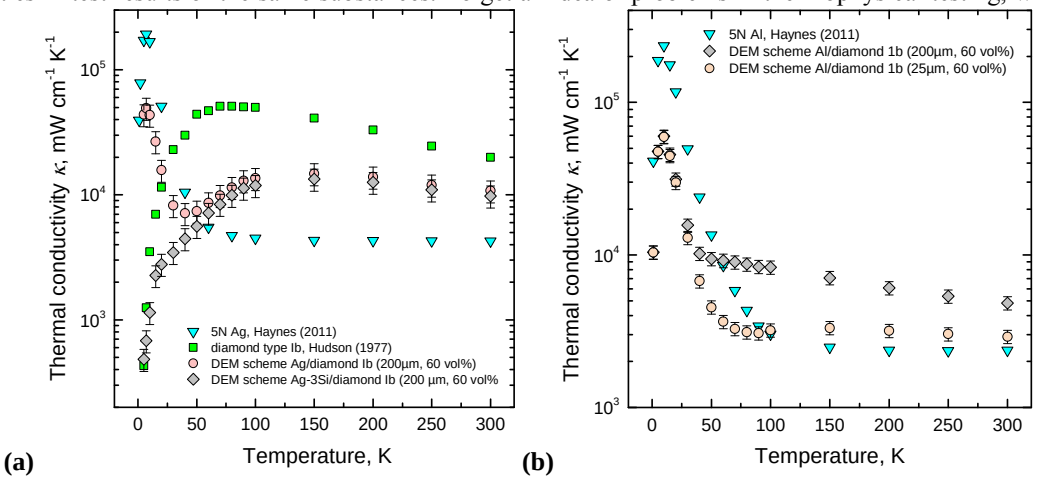


**Figure 3. (a) Evolution of the thermal conductivity $\kappa$(T) according DEM approach for Ag/diamond and Ag-3Si/diamond composites with 200 µm sized diamonds (approx. mesh 70/80, 60 v%) compared to the pure substances 5N Ag [1] and diamond Ib [2] in the temperature range 4 K < T < 300 K. *h* values for calculations according Eq. (1) are from [3], $\kappa_m$ of Ag-3Si from Figure 5b. (b) displays calculations of $\kappa$(T) for Al/diamond composites considering two different sizes of diamonds, 200 µm and 25 µm.**

The remarkable feature of Figure 3 is that the DEM-scheme calculation of $\kappa$(T) for Ag/diamond splits in two sections: in the first, at low temperatures, $\kappa_c$(T) follows $\kappa_m$(T) of the (pure) metallic matrix. Although both peaks are at roughly the same temperature, the composite thermal conductivity is lower, as rather high scattering rates on static imperfections can be assumed owing to the presence of diamonds.

Thermal conductivity in the second section, at higher temperatures, is dominated by the intrinsic conductivity of diamonds and the peak is displaced to a higher temperature compared to the maximum in thermal conductivity for pure diamond. This second composite conductivity maximum is again lower than the pure substance.

When soluble elements (like Si in Ag [36]) are present, the low temperature maximum in $\kappa$(T) diminishes due to severe scattering effects. When including experimental values of $\kappa_m$(T) for Ag–3Si (see section C, Figure 5a) in the DEM-calculations, the low temperature maximum in $\kappa_c$(T) of Ag–3Si/diamond (Figure 3) disappears, although the second section, roughly above 60 K, nearly coincides with $\kappa_c$(T) of pure Ag/diamond.

In consequence to the above it is clear that the use of pure matrices is favorable for $\kappa_c$(T). On the other hand, it must be clear, that *) up to now no successful infiltrations of diamonds with pure Ag are reported (due to bad wetting behavior) and **) such calculations reflect ideal conditions and do not consider necessary interfacial conditions like the necessary bonding between the constituents and which is hard to fulfill by a pure Ag-matrix, as no mutual reactivity exists. Consequently, $\kappa_c$(T) of pure Ag/diamond composites will hardly match with the above presented DEM-calculations.

Figure 3b displays the calculations for $\kappa_c$(T) of pure Al/diamond when considering diamonds of two different sizes, i.e. 200 µm and 25 µm (roughly mesh 500/600) and again assuming a volume fraction of 60 %. The calculations clearly show the dependence of thermal conductivity on diamond particle sizes. Although Equation (1) purports such behavior, interestingly, this size dependence is noticeable solely at temperatures above 30 K. Below, the graphs for 200 µm and 25 µm coincide. Furthermore, an ambient thermal conductivity close to pure Al is predicted for Al/25µm diamond composites, indicating, that the use of very small size inclusions can be detrimental to thermal conductivity in composites. When increasing the particle size to 200 µm, ambient thermal conductivity is predicted to nearly double compared to an unreinforced Al-matrix.

### B. Clean model system: characterization of surface termination

XPS spectra were taken on 3 mm × 3 mm diamonds with each different surface treatment. Apart from O and C no significant contaminations (> 0.5 at%) were found in the survey spectra. Figure 4a shows the recorded XPS signal of the C 1s core peaks of diamond as a function of sample surface treatment. In order to estimate the content of $sp^3$, $sp^2$ and oxidized carbon species, de-convolution of the C 1s peaks was performed using three Gaussian-

Lorentzian curves (Figure 4b for aqua regia treated diamond). The main peak is located at a binding energy of 285.2 eV and attributed to $sp^3$ carbon. The one at higher binding energies i.e. at 286.7 eV may be attributed to C-O surface termination and/or C-H surface termination. The latter has been reported to occur at 0.7 to 1.0 eV higher binding energies than the $sp^3$ carbon species on well-defined boron doped diamond surfaces[37]. The third carbon species is located at lower binding energies (i.e. 284.2 eV) than the main peak and is attributed to $sp^2$ carbon.

Table 1 depicts the analysis of the carbon and oxygen content as well as the amount of carbon species derived from de-convolution of the angle integrated C 1s signals.

**Table 1:** Results of the angle integrated quantitative analysis of the recorded XPS signals.

| Component, at% | H terminated | $H_2SO_4$ | aqua regia |
|---|---|---|---|
| **C** | 93.7 | 91.9 | 91.4 |
| **O** | 6.3 | 8.1 | 8.6 |
| **C $sp^3$** | 81.7 | 80.7 | 84.1 |
| **C $sp^2$** | 14.7 | 13.9 | 7.6 |
| **C-O/C=O/C-H** | 3.7 | 5.5 | 8.3 |

The amount of oxygen is lowest for the H-terminated sample and shows a significant increase after acid treatment. The amount of $sp^3$ carbon is highest for aqua regia treatment and decreases with increasing angle and therewith surface sensitivity (Figure 4c). Oxygen, $sp^2$ carbon as well as C-O and/or C-H species are located at the outer layers of the surface, respectively. Interestingly, the proportion of $sp^2$ bonds is highest when H terminated and lowest for aqua regia treatment. The $H_2SO_4$ sample has a proportion of $sp^2$ bonds close to the H terminated one. The integrated C 1s core peak analysis (Table 1) shows less oxygen for the H-terminated sample compared to the $H_2SO_4$ and the aqua regia terminated ones. The low oxygen concentration confirms a decrease of surface oxygen upon the H-treatment.

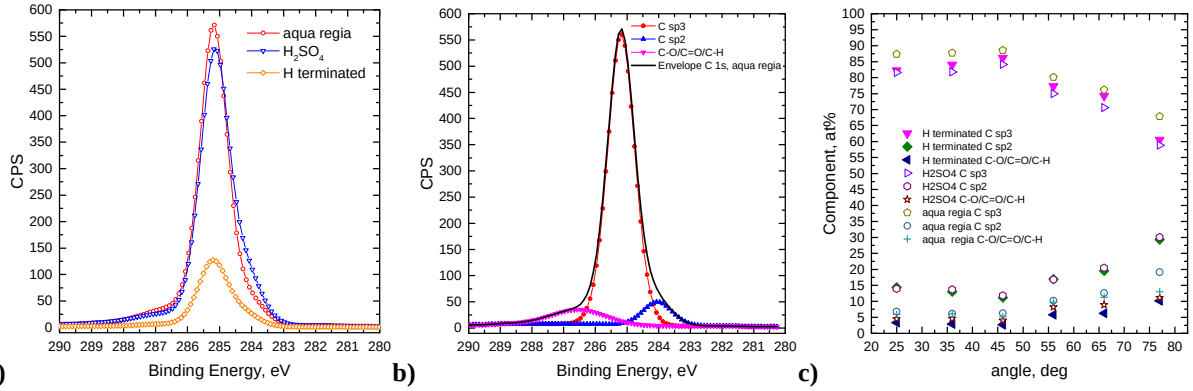


**Figure 4 a) XPS raw curves and their envelope fits around the C 1s peak of diamond as a function of sample surface treatment. b) De-convolution procedure of the recorded C 1s core peak of aqua regia treated diamond. c) angle resolved quantitative analysis of the recorded C 1s signals**

The angle resolved analysis indicates the highest amount of surficial oxygen (approx. 14.5 at%) and C-O bonds (11.1 at%) for the aqua regia surface treated diamond close to an emission angle of 77° with respect to the surface normal. C-O bonds generally decrease with steeper angle for all different treatments. The observation that the $H_2SO_4$ treated sample shows equal amount of oxygen, but less C-O species if compared to the aqua regia treated one, may be explained by small residues of sulfate on the surface as approximately 0.5 at% of Sulphur were detected in the survey spectra. The quantity of $sp^2$-bonds increases upon an increasing emission angle, as for every non $sp^3$ carbon species.

The results of the XPS measurements can be summed up as follows:

- The detected signals of all non-$sp^3$-carbon species increase with increasing emission angle, confirming that they are only present at the uppermost atomic layers of the diamond.
- The H-treatment leads to decreased amounts of both oxygen and C-O bonds.
- The $sp^3$ amounts are largely comparable, the $sp^2$ amounts show notable differences, with the highest amount for the H-terminated diamond surface and the lowest for the aqua regia treated one.

XPS results presented above, are largely in line with former contact angle measurements of water on surface terminated diamond monocrystals[38] and AFM force-distance curve experiments[26]. They confirm that H termination

results in strong adhesion to the tip and diminishes for an oxygen terminated surface. These changes in the adhesive force may be attributed to the different surface terminations. Upon surface termination the contact angle changes indicating hydrophilic surface by $H_2SO_4$ treatment and hydrophobic surface by aqua regia treatment. A decrease in contact angle in between both terminations may be explained by the introduction of oxygen terminations upon the $H_2SO_4$ treatment and thus an increase in hydrophilicity.

### C. Matrix thermal conductivity $\kappa_m$(T) between 4 K and ambient

The thermal conductivities of unreinforced matrix samples of Ag–0.5Si, Ag–1Si, and the eutectic Ag–3Si alloys

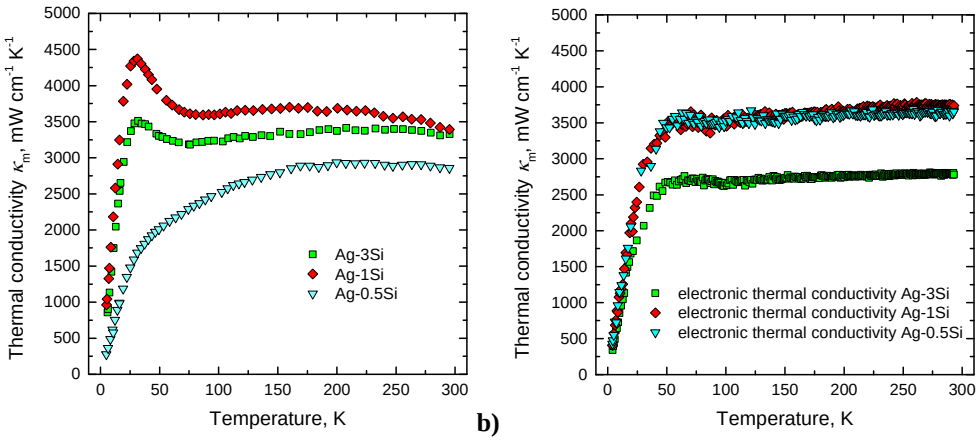


**Figure 5. (a) Matrix thermal conductivity $\kappa_m$(T) from steady-state heat flow experiment, and (b) electronic thermal conductivity $\kappa_m$(T) for Ag-3Si, Ag-1Si and Ag-0.5Si calculated via the Wiedemann-Franz law from electrical resistivity data. All alloys are heat treated at 830 °C/2 h and 500 °C/20 h before measuring $\kappa$(T).**

as a function of the temperature between 4 K and ambient temperature are displayed in Figure 5. Experimentally, thermal conductivity was defined by the steady state heat flow method described in section II of this text and recording electrical resistivity, respectively. Hence electronic thermal conductivity is calculated applying Wiedemann-Franz law to electrical resistivity data.

Note, that $\kappa_m$(T) data of pure Ag are not displayed in Figure 5, as it has not yet been possible to produce MMCs with pure silver matrix by LMI. The wetting behavior between diamond and pure silver is obviously unfavorable in such, that even a high gas pressure of 150 bar is not adequate to force the liquid silver into the diamond particle beds. Even small additions of Si in Ag significantly change the wetting behavior, thus being able to produce Ag/diamond MMCs. Furthermore, it is important to know, that heat treatment is essential, as the thermal conductivity behavior significantly changes between as-cast and heat treated conditions [38]. Hence, data presented in Figure 5 and Figure 6 are from heat treated state.

Graphs for thermal conductivity in Figure 5a and b differ considerably: Ag–1Si and Ag–3Si exhibit thermal conductivity maxima at roughly 30 K and determined by the steady state heat flow method, whereas the graphs for electronic thermal conductivity in Figure 5 b) do not show such maxima. Furthermore, the thermal conductivity and the electronic thermal conductivity of Ag–0.5Si and Ag–3Si are quite different at temperatures between 50 K and ambient. The electronic thermal conductivity suggests an ambient conductivity of 2800 mW cm$^{-1}$ K$^{-1}$ for Ag–3Si, roughly 3600 mW cm$^{-1}$ K$^{-1}$ for Ag–1Si and Ag–0.5Si, whereas the experimental data from the

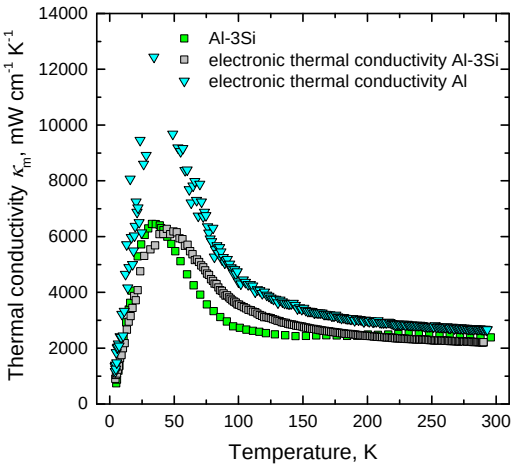


**Figure 6. $\kappa_m$(T) of Al and Al–3Si alloy from steady-state heat flow experiment and electronic thermal conductivity calculated via the Wiedemann-Franz law from electrical resistivity data. The alloy is initially heat treated at 550 °C/2h and 250 °C/12h before conductivity and resistivity testing.**

steady state method give 2900 mW cm$^{-1}$ K$^{-1}$ for Ag–0.5Si and nearly 3400 mW cm$^{-1}$ K$^{-1}$ for Ag–3Si and Ag–1Si.

We conclude that this may be ascribable to the contribution of thermally high, but electrically low conductive Si particles in the Ag–Si matrix, thus contributing higher to the thermal conductivity, but not contributing to the electrical conductivity. Strictly speaking Wiedemann-Franz law is not (or very limited) applicable for composite materials. As Ag–Si has (almost) no mutual solubility at ambient temperature, it must be largely treated as a composite, consisting of two different electrically and thermally conductive phases Ag and Si, respectively. Furthermore, small

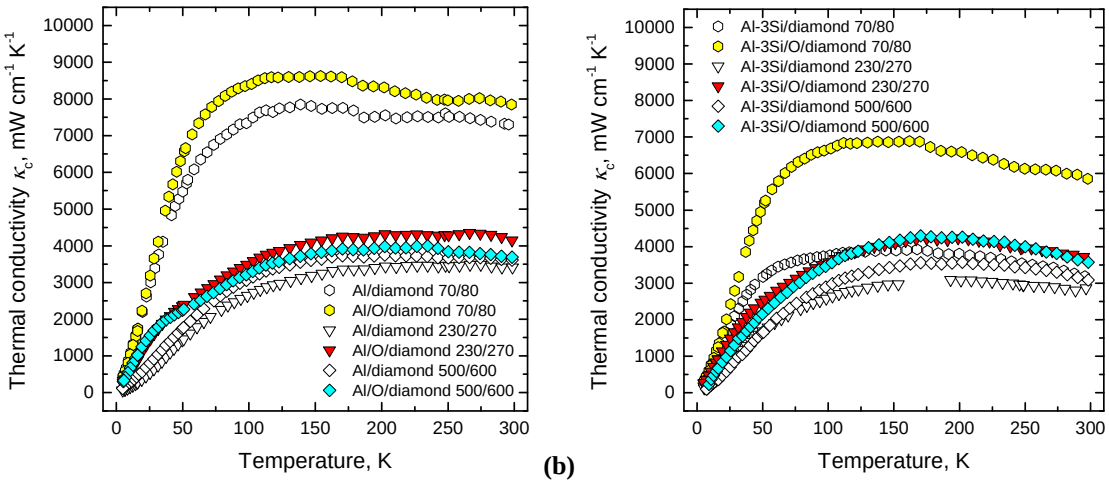


**Figure 7. $\kappa_c$(T) of (a) Al/diamond and (b) Al–3Si/diamond composites using mesh 70/80, 230/270 and 500/600 diamonds. Al–Si composites are heat treated at 550 °C/2h and 250 °C/12h prior to the thermal conductivity measurements, except pure Al/diamond MMCs, which are not in a heat treated condition.**

quantities of residual dissolved Si in Ag must be considered [39] and such solid solution may behave different in thermal conductivity and electrical resistivity.

The eutectic Ag–3Si alloy contains roughly 11–12 vol.% Si particles which reduce the electrical conductivity by some 20 %. This also goes hand in hand with a $\kappa_m$(T) maximum in experimental thermal conductivity data of Ag–3Si at roughly 30 K, which is not visible in the calculated electronic conductivity, reflecting again the different contributions of Si to the electrical and thermal conductivity. Interestingly, above discussed differences between electronic thermal conductivity and thermal conductivity are almost negligible in Al–Si, Figure 6.

Based on the results for $\kappa_m$(T) measurements we selected pure Al, Al–3Si, Ag–1Si, and Ag–3Si nominal compositions for subsequent MMC preparation and $\kappa_c$(T) measurements, see section D.

### D. Composite thermal conductivity $\kappa_c$(T) and interface thermal conductance $h$(T) between 4 K and ambient

Figure 7 shows the results obtained for the composite thermal conductivity $\kappa_c$ as a function of temperature for both matrix systems Al and Al–3Si with different diamond particle sizes surface terminated (oxygenated, and H-terminated). Interestingly the maximum obtained for pure Al at roughly 30 K (Figure 6) disappears in all Al/diamond composites and may be attributed to rather high scattering on static imperfections.

As predicted by Equation (1) and Figure 3b, $\kappa_c$(T) depends on inclusion size with in general higher conductivities with larger diamonds. Compared to the ambient temperature thermal conductivity of pure Al, which is in the order of 2650 mW cm$^{-1}$ K$^{-1}$ (Figure 6), we can deduce significant enhancement in thermal conductivity for all composites, but least increase for the smallest sized diamonds (500/600 mesh) (+ 45%) and highest for the largest diamonds (70/80 mesh) (+ 175%). Upon using Al–3Si instead of pure Al, thermal conductivity behavior of the composites significantly changes, Figure 7b. The influence of diamond size is somehow negligible when approaching ambient temperature but can be distinct at lower temperatures. Close to ambient temperature the increase in conductivity compared to the unreinforced matrix is rather small, i.e. between + 16% and + 30%.

There is a further increase in thermal conductivity in the overall temperature range upon oxygenation of the diamonds, for both systems Al/diamond and Al–3Si/diamond. This increase is extremely pronounced for Al–3Si/O/diamond 70/80, where the increase is roughly + 150% compared to the unreinforced sample and + 90% compared to the H-terminated sample Al–3Si/diamond 70/80. However, the highest composite thermal conductivity is about 8500 mW cm$^{-1}$ K$^{-1}$ at 100 to 150 K for Al/O/diamond 70/80, Figure 7a. This is in line with XPS results, as by

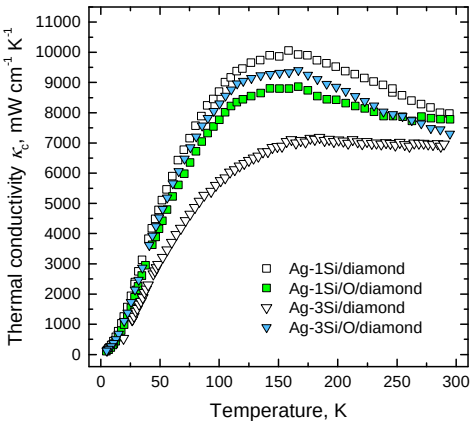


**Figure 8. Ag–1Si/diamond and Ag–3Si/diamond composites using O and H terminated mesh 70/80 diamonds. The materials are heat treated at 830 °C/2h and 500 °C/20h (Ag–Si) prior to the thermal conductivity measurements**

aqua regia treatment obviously the quantities of surficial oxygen and C-O bonds drastically increase compared to an H terminated sample, hence bonding and phonon-electron coupling at the interfaces between metallic matrix and diamonds are greatly enhanced.

In the Ag/diamond system, Figure 8, thermal conductivity at ambient temperature can increase drastically compared to the unreinforced Ag–Si matrix by a factor of 2.4. Note, that the influence of diamond sizes in the Ag–Si/diamond system is described in detail elsewhere [40]. Interestingly the influence of surface termination is pronounced for Ag–3Si, in Ag–1Si thermal conductivity decreases upon using oxygenated diamonds. The highest measured conductivity was in the Ag–1Si/diamond sample and reaches 10000 mW cm$^{-1}$ K$^{-1}$ at roughly 150 K. This is quite close to the predictions by the DEM-model in Figure 3a. Modeling and experimental data almost coincide at temperatures between 4 K and roughly 150 K, but can, however, differ when approaching ambient temperature. Those calculations predict an ambient thermal conductivity of nearly 10800 mW cm$^{-1}$ K$^{-1}$ for pure Ag/diamond and 9800 mW cm$^{-1}$ K$^{-1}$ for Ag–3Si/diamond, respectively, whereas the experimental data reveal 8000 mW cm$^{-1}$ K$^{-1}$ as its highest for Ag–1Si/diamond.

Both, Ag–1Si and Ag–3Si show no maxima in $\kappa_c$(T) at 30 K, as $\kappa_m$(T) for the matrix in Figure 5a suggests. Again, this may be attributed to scattering effects by the presence of diamonds.

However, this is in line with DEM calculations in Figure 3a, when considering experimental data for Ag–3Si matrix, hence, the DEM predictions are in rather close agreement to the experimental data for the composite in Figure 8.

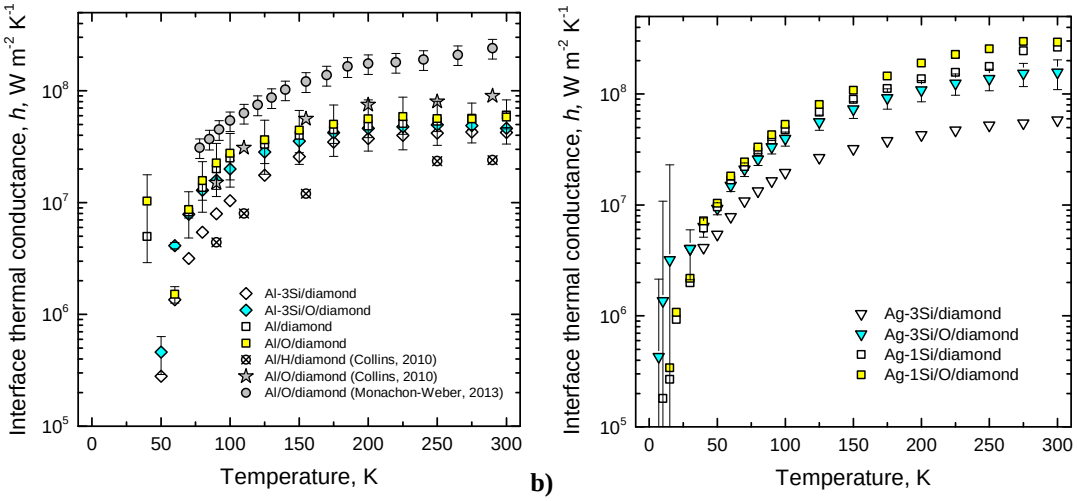


**a)** **b)**

**Figure 9. Interface thermal conductance *h*(T) of (a) Al–xSi/diamond composites and (b) Ag–xSi/diamond composites, calculated from the effective conductivities using Eq. (2). Data for Al composites are compared with *h*(T) results given by Monachon [8] and Collins [12] on model interfaces in TDTR experiments.**

Figure 9 shows the calculated interface thermal conductance $h$(T), deduced from the linear plots of $1/\kappa_d^{eff}$(T) versus $1/a$. Errors arise from calculation uncertainties within the linear approximation, as small fluctuations in $\kappa_d^{eff}$ can even cause negative $h$-values, for which large error bars are plotted in Figure 9 at temperatures < 50 K.

We further notice almost negligible differences in $h$(T) between Al/diamond and Al/O/diamond composites, but more distinctive difference in the Al–3Si system at lower temperatures. In the Ag–3Si and Ag–1Si systems, Figure 9b, we can see a clear influence of oxygenation for Ag–3Si, but this effect is very less pronounced for Ag–1Si.

When comparing our data for Al/diamond with those obtained by Collins[13] and Monachon[3], we can identify a clear disagreement and which can be attributed to the use of a clean model system (i.e. sputtered layer on diamond mono crystals) in the TDTR experiments and composites fabricated under typical messier lab-scale conditions of gas pressure infiltration. The experimental data in our findings are roughly a factor of 2.5 higher than those obtained by Collins[13] in the H terminated Al/diamond system. Conversely, we see much higher values for the oxygenated samples obtained by Monachon[3] than in our findings. For Ag–3Si and Ag–1Si we can only compare ambient temperature values from TDTR measurements in the Ag–diamond system[9]: the interface thermal conductance of $6 \pm 1 \times 10^7$ $Wm^{-2}$ $K^{-1}$ obtained by Tavangar[9] is in agreement with our findings shown in Figure 9b for the Ag–3Si/diamond system. There is, however, a marked increase in *h*, roughly a factor of 5, between Ag–3Si/diamond, Ag–1Si/diamond and Ag–1Si/O/diamond composites, and a factor of 3 between the oxygenated and H-terminated samples in the Ag–3Si system.

### E. Diamond composites and laser crystals

Brazing of laser crystals to a heat sink can cause delamination effects, as the heat sink (commonly pure copper) and a laser crystal can have highly different coefficients of thermal expansion. Resulting stresses may destroy the slab crystal. Depending on inclusion volume fraction, a diamond composite can have low CTE. Typically, this is in the range of 8-12 ppm $K^{-1}$ at ambient temperature. To give an idea of typical CTEs of two important laser crystal materials, the CTE of $CaF_2$ is about 19, the CTE of $YLiF_4$ is anisotropic, i.e. about 13 ppm $K^{-1}$ along a-axis and 8 ppm $K^{-1}$ along c-axis.

In this approach, two selected laser crystal materials were directly joined to a diamond composite while performing the infiltration process of liquid Al- and Ag-alloys in diamond beds. The laser crystal materials were placed inside a graphite die and cavities were filled up with diamond particles (Figure 10a). The subsequent process of infiltration was performed in the same way like for all composites and described in the experimental section. However, the crystals have to withstand high temperatures and possible thermal shocks during the infiltration process.

In a first approach we used $CaF_2$ and $YLiF_4$ crystals of either cylindrical or rhombic shape. Ideally the laser crystals should protrude approx. 1 to 2 mm from the surface of the MMC to ensure free-standing faces of the crystal to ensure the pumping in a double-side, double-pass configuration. Alternatively, the slab crystal is a cylinder being encased by the MMC and having two transmissive open ends. However, once the different concepts are proven, different geometries and designs should be easily realizable.

First a rhombic $CaF_2$-crystral was embedded in a AgSi1/diamond MMC (Figure 10b). Cracks are visible within

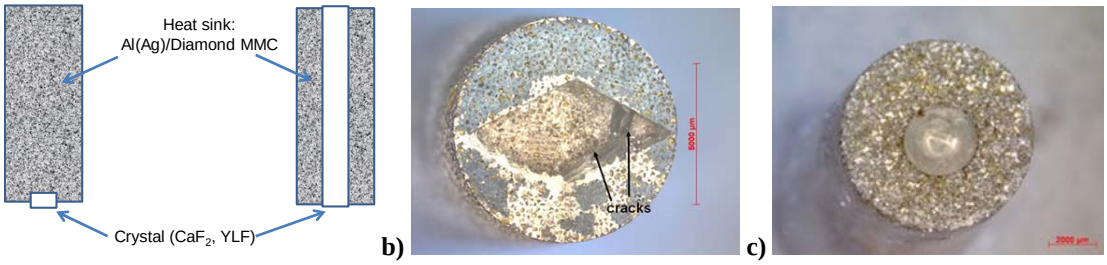


**Figure 10: a) Generic designs of $CaF_2$ and $YLiF_4$ crystals in Al-, or Ag-MMC heat sinks. b) $CaF_2$ crystal embedded in Ag-1Si/diamond, and c) $YLiF_4$ slab crystal in eutectic Al-12.6Si/diamond heat sink**

the crystal, which may be due to the high temperature necessary for infiltrating with a Ag-based alloy and by differences in CTE between the MMC and the crystal, respectively. As an alternative we used $YLiF_4$ instead of $CaF_2$. As the CTE of $YLiF_4$ is lower than $CaF_2$, the use of a diamond MMCs with adaptable CTE may exclude crack induced by the largely different CTEs. However, a main drawback of the proposed concept is the relatively low melting point of $YLiF_4$ of 825 °C, thus excluding the application of Ag–Si/diamond composites. We therefore investigated low melting eutectic Al–12.6Si matrix alloys and diamonds as MMC heat sink (Figure 10c). No cracks are visible in the $YLiF_4$-crystal, even after dis-embedding the crystal by dissolving the matrix and removing the crystal (Figure 10c). Investigations are at an early stage, future investigations may concern the use of alternative slab crystal materials like YAG, the measurement of the overall CTE of the hybrids and to clarify advantages/disadvantages of such processing.

## IV. Conclusion

Plane diamond substrates as clean model system were functionalized, i.e. hydrogenated and oxygenated respectively. XPS investigations show that the H-treatment leads to decreased amounts of both oxygen and C-O bonds. Furthermore, the $sp^2$ amounts show notable differences, with the highest amount for the H-terminated diamond surface and the lowest for the aqua regia treated one.

Thermal conductivity of Al/diamond, Al–3Si/diamond, Ag–xSi/diamond composites and their respective matrix alloys was investigated as a function of temperature by a steady state heat flow method. Furthermore, electrical resistivity measurements of matrix alloys were performed to calculate electronic thermal conductivity $\kappa_e$. Interestingly, there is a marked difference between the two methods for Ag–xSi alloys, as the steady state method shows distinct maxima in $\kappa_m(T)$ at roughly 30 K for Ag–3Si and Ag–1Si, but not in $\kappa_e(T)$, the electronic thermal conductivity. Furthermore, the ambient thermal conductivity values differ significantly. This is ascribable to the contribution of thermally high, but electrically low conductive Si particles in the Ag–Si matrix, thus contributing higher to the thermal conductivity, but not contributing to the electrical conductivity. This effect is minor in the Al–Si system.

Composite thermal conductivity measurements show a dependence from diamond particle size, matrix composition and diamond oxygenation: the larger the diamonds, the higher thermal conductivity, and, in Al and Al–3Si the use of oxygenated diamonds can drastically increase $\kappa_c(T)$. $\kappa_c$ was highest for Ag–1Si/diamond 70/80 (around 10000 mW $cm^{-1}$ $K^{-1}$ at roughly 150 K), and 8500 mW $cm^{-1}$ $K^{-1}$ at 100 to 150 K for Al/O/diamond 70/80.

Predictions of thermal conductivity $\kappa_c(T)$ by DEM scheme are in rather close agreement to the experimental data for composites of the Ag–3Si system. For the Al system a distinct maximum in $\kappa_c(T)$ is predicted but experimentally not verifiable, as the diamond inclusions obviously cause scattering. The inverse method allows calculating the thermal boundary conductance $h(T)$ and showed a significant increase in conductance upon oxygenation of diamonds in the Ag–3Si system. In the Al/diamond system this effect is small, although there is a factor of roughly 2.5 in $h$ between Al/diamond and Al–3Si/diamond. $YLiF_4$ laser crystals were successfully embedded in an Al/diamond heat sink material.

## Acknowledgments

Part of this work was supported financially by ESA/ESTEC, The Netherlands (contract 4000105706/12/NL/CBi).

## References

[1]Haynes, W. M., and Lide, S. r. CRC Handbook of Chemistry and Physics.). CRC Press, Boca Raton, FL, 2011-2012.
[2]Hudson, P. R. W., and Phakey, P. P., "Defects in natural type IB diamond", *Nature*, Vol. 269*,* 1977, pp. 3.
[3]Monachon, C., and Weber, L., "Influence of diamond surface termination on thermal boundary conductance between Al and diamond", *Journal of Applied Physics*, Vol. 113*,* 2013.
[4]Ott, M. N., Coyle, D. B., Canham, J. S., and Leidecker, H. W., "Qualification and Issues with Space Flight Laser Systems and Components", *Proceedings of Lasers and Applications in Science and Engineering, Solid State Lasers XV: Technology and Devices, SPIE 6100*, edited by Hoffman, H. J. and Shori, R. K., International Society for Optics and Photonics, 2006.
[5]Naidich, Y. V., and Kolesnichenko, G. A., "Study of the wetting of diamond and graphite by liquid metals", *Powder Metallurgy and Metal Ceramics*, Vol. 2*,* 1964, pp. 35-38.
[6]Scott, P. M., Nicholas, M., and Dewar, B., "The wetting and bonding of diamonds by copper-base binary alloys", *Journal of Materials Science*, Vol. 10*,* 1975, pp. 1833-1840.
[7]Schubert, T., Trindade, B., Weißgärber, T., and Kieback, B., "Interfacial design of Cu-based composites prepared by powder metallurgy for heat sink applications", *Materials Science and Engineering: A*, Vol. 475*,* 2008, pp. 39-44.
[8]Neubauer, E., Kladler, G., Eisenmenger-Sittner, C., et al., "Interface design in copper-diamond composite by using PVD and CVD coated diamonds", *Advanced Materials Research*, Vol. 59*,* 2009, pp. 214-219.
[9]Tavangar, R., Molina, J. M., and Weber, L., "Assessing predictive schemes for thermal conductivity against diamond-reinforced silver matrix composites at intermediate phase contrast", *Scripta Materialia*, Vol. 56*,* 2007, pp. 357-360.
[10]Ruch, P. W., Beffort, O., Kleiner, S., Weber, L., and Uggowitzer, P. J., "Selective interfacial bonding in Al(Si)–diamond composites and its effect on thermal conductivity", *Composites Science and Technology*, Vol. 66*,* 2006, pp. 2677-2685.
[11]Edtmaier, C., Weber, L., and Tavangar, R., "Surface Modification of Diamonds in Diamond/Al-Matrix Composite", *Advanced Materials Research*, Vol. 59*,* 2009, pp. 125-130.
[12]Johnson, W. B., and Sonuparlak, B., "Diamond/Al metal matrix composites formed by the pressureless metal infiltration process", *Journal of Materials Research*, Vol. 8*,* 1993, pp. 1169-1173.
[13]Collins, K. C., Chen, S., and Chen, G., "Effects of surface chemistry on thermal conductance at aluminum–diamond interfaces", *Applied Physics Letters*, Vol. 97*,* 2010, pp. 083102.

[14]Monachon, C., and Weber, L., "Thermal boundary conductance of transition metals on diamond", *Emerging Materials Research*, Vol. 1*,* 2012, pp. 89-98.
[15]Silvain, J.-F., Veillere, A., Heintz, J.-M., et al., "The role of controlled interfaces in the thermal management of copper-carbon composites", *Emerging Materials Research*, Vol. 1*,* 2012, pp. 75-88.
[16]Mortimer, A., and Nicholas, M., "The Wetting of Carbon by Copper and Copper Alloys", *Journal of Materials Science*, Vol. 5*,* 1970, pp. 149-155.
[17]DeVincent, S. M. "Development of Graphite/Copper Composites Utilizing Engineered Interfaces", Cleveland, Ohio, NASA Contractor Report 187143, 1991.
[18]Collins, K. C., Chen, S., and Chen, G., "Effects of surface chemistry on thermal conductance at aluminum--diamond interfaces", *Applied Physics Letters*, Vol. 97*,* 2010, pp. 083102.
[19]Monachon, C., Schusteritsch, G., Kaxiras, E., and Weber, L., "Qualitative link between work of adhesion and thermal conductance of metal/diamond interfaces", *Journal of Applied Physics*, Vol. 115*,* 2014, pp. 123509.
[20]Stoner, R. J., Maris, H. J., Anthony, T. R., and Banholzer, W. F., "Measurements of the Kapitza conductance between diamond and several metals", *Physical Review Letters*, Vol. 68*,* 1992, pp. 1563-1566.
[21]Lyeo, H.-K., and Cahill, D. G., "Thermal conductance of interfaces between highly dissimilar materials", *Physical Review B*, Vol. 73*,* 2006, pp. 144301.
[22]Gundrum, B. C., Cahill, D. G., and Averback, R. S., "Thermal conductance of metal-metal interfaces", *Physical Review B*, Vol. 72*,* 2005, pp. 245426.
[23]Stoner, R. J., and Maris, H. J., "Kapitza conductance and heat flow between solids at temperatures from 50 to 300 K", *Physical Review B*, Vol. 48*,* 1993, pp. 16373-16387.
[24]Monachon, C., and Weber, L., "Effect of diamond surface orientation on the thermal boundary conductance between diamond and aluminum", *Diamond and Related Materials*, Vol. 39*,* 2013, pp. 8-13.
[25]Kida, M., Weber, L., Monachon, C., and Mortensen, A., "Thermal conductivity and interfacial conductance of AlN particle reinforced metal matrix composites", *Journal of Applied Physics*, Vol. 109*,* 2011, pp. 064907.
[26]Edtmaier, C., Bauer, E., Weber, L., Tako, Z. S., Segl, J., and Friedbacher, G., "Temperature dependence of the thermal boundary conductance in Ag–3Si/diamond composites", *Diamond and Related Materials*, Vol. 57*,* 2015, pp. 37-42.
[27]Segl, J., and Edtmaier, C., "Influence of the diamond surface termination on the thermal conductivity of Al/diamond- and Ag/diamond MMCs", *Materials Science Forum*, Vol. 825-826*,* 2015, pp. 142-149.
[28]Mérel, P., Tabbal, M., Chaker, M., Moisa, S., and Margot, J., "Direct evaluation of the sp3 content in diamond-like-carbon films by XPS", *Applied Surface Science*, Vol. 136*,* 1998, pp. 105-110.
[29]Atchison, F., Bryś, T., Daum, M., et al., "Structural characterization of diamond-like carbon films for ultracold neutron applications", *Diamond and Related Materials*, Vol. 16*,* 2007, pp. 334-341.
[30]Shirley, D. A., "High-Resolution X-Ray Photoemission Spectrum of the Valence Bands of Gold", *Physical Review B*, Vol. 5*,* 1972, pp. 4709-4714.
[31]Scofield, J. H., "Hartree-Slater subshell photoionization cross-sections at 1254 and 1487 eV", *Journal of Electron Spectroscopy and Related Phenomena*, Vol. 8*,* 1976, pp. 129-137.
[32]White, G. K., "Thermal Conductivity of Silver at Low Temperatures", *Proceedings of the Physical Society A*, Vol. 66*,* 1953, pp. 844-845.
[33]Woodcraft, A. L., "Recommended values for the thermal conductivity of aluminium of different purities in the cryogenic to room temperature range, and a comparison with copper", *Cryogenics*, Vol. 45*,* 2005, pp. 626-636.
[34]Woodcraft, A. L., "Predicting the thermal conductivity of aluminium alloys in the cryogenic to room temperature range", *Cryogenics*, Vol. 45*,* 2005, pp. 421-431.
[35]Pintsuk, G., Blumm, J., Hohenauer, W., et al., "Interlaboratory Test on Thermophysical Properties of the ITER Grade Heat Sink Material Copper–Chromium–Zirconium", *International Journal of Thermophysics*, Vol. 31*,* 2010, pp. 2147-2158.
[36]Weber, L., "Equilibrium Solid Solubility of Silicon in Silver", *Metallurgical and Materials Transactions A*, Vol. 33*,* 2002.
[37]Diederich, L., Küttel, O. M., Aebi, P., and Schlapbach, L., "Electron affinity and work function of differently oriented and doped diamond surfaces determined by photoelectron spectroscopy", *Surface Science*, Vol. 418*,* 1998, pp. 219-239.
[38]Edtmaier, C., Bauer, E., Tako, Z. S., et al. "Thermal conductivity behavior of Ag-, and Al-diamond composites for heat sink applications in the temperature range 4 K < T < 298 K," *Proccedings of 13th European Conference on Spacecraft Structures, Materials & Environmental Testing, Braunschweig, Germany,* 2014.
[39]Weber, L., "Equilibrium solid solubility of silicon in silver", *Metallurgical and Materials Transactions A*, Vol. 33*,* 2002, pp. 1145-1150.
[40]Edtmaier, C., Bauer, E., Tako, Z. S., and Segl, J., "Thermal conductivity behaviour of Al/diamond and Ag/diamond composites in the temperature range 4 K < T < 293 K", *Materials Science Forum*, Vol. 825-826*,* 2015, pp. 197-204.